frontiers in Materials

ORIGINAL RESEARCH
published: 16 March 2021
doi: 10.3389/fmats.2021.645612

Effect of Y_2O_3 Addition on High-Temperature Oxidation of Binderless Tungsten Carbide

Jinfang Wang[1,2,3], Dunwen Zuo[1], Liu Zhu[2,3]*, Zhibiao Tu[2], Xiao Lin[4], Yinan Wu[5], Weiwei Li[2] and Xiaoqiong Zhang[2]*

[1]College of Mechanical and Electrical Engineering, Nanjing University of Aeronautics and Astronautics, Nanjing, China, [2]School of Pharmaceutical and Materials Engineering, Taizhou University, Taizhou, China, [3]Zhejiang Provincial Key Laboratory for Cutting Tools, Taizhou, China, [4]Zhejiang Crystal-Optech Co. LTD, Taizhou, China, [5]Taizhou Product Quality and Safety Inspection Institute, Taizhou, China

High-temperature oxidation tests were carried out on binderless tungsten carbide (WC) with different Y_2O_3 contents (0, 1, 2, 3, and 4 wt.%) and on YG3 cemented carbide. Results demonstrated that the addition of Y_2O_3 led to a significant improvement in the high-temperature oxidation resistance of binderless tungsten carbide compared with those of YG3 cemented carbide and pure tungsten carbide. After oxidation at 800°C for 120 min, the oxidation weight gain of binderless tungsten carbide with 1 wt.% Y_2O_3 was 58.54 mg cm^{-2}, corresponding to the reduction by 47.7% compared with YG3 cemented carbide. In the high temperature oxidation process, WC in the triangle grain boundary was first oxidized to Y_2WO_6 due to the high activity of Y_2O_3 which is present mainly in the WC grain boundaries. The transport of W^{4+} outward along the grain boundary and the diffusion of O^{2-} inward along the grain boundary were hindered by Y_2WO_6 with the high ionic radius and thus the antioxidant capacity of binderless tungsten carbide was improved. Meanwhile, the adhesive ability of oxidation layer on the substrate was enhanced with the "pinning effect" of Y_2WO_6, which also led to the improvement of oxidation resistance. With the Y_2O_3 content increasing from 1 to 4 wt.%, the antioxidant properties of binderless tungsten carbide gradually declined, and the antioxidant performance of binderless tungsten carbide with 1 wt.% Y_2O_3 was found to be the best.

Keywords: high-temperature oxidation, Y_2O_3, binderless, tungsten carbide, oxidation kinetics

OPEN ACCESS

Edited by:
Antonio Caggiano, Darmstadt University of Technology, Germany

Reviewed by:
Haibin Wang, Beijing University of Technology, China
Hao Lu, Beijing University of Technology, China
Kaihua Shi, Zigong Cemented Carbide Co., Ltd., China

****Correspondence:***
Dunwen Zuo
imit505@nuaa.edu.cn
Liu Zhu
zhuliu@tzc.edu.cn

Specialty section:
This article was submitted to Structural Materials, a section of the journal Frontiers in Materials

Received: *23 December 2020*
Accepted: *05 February 2021*
Published: *16 March 2021*

Citation:
Wang J, Zuo D, Zhu L, Tu Z, Lin X, Wu Y, Li W and Zhang X (2021) Effect of Y_2O_3 Addition on High-Temperature Oxidation of Binderless Tungsten Carbide. Front. Mater. 8:645612. doi: 10.3389/fmats.2021.645612

INTRODUCTION

Tungsten carbides with metallic binder cobalt are widely used for cutting tools and wear applications due to their excellent mechanical properties (Kim et al., 2004; Xiao et al., 2010; Ou et al., 2012; Zhang et al., 2016; Liu et al., 2018). Although the binder cobalt greatly improves sinter ability and fracture toughness, they also weaken the hardness, wear resistance, and corrosion resistance of WC matrix, especially at high temperatures (Engqvist et al.,1999; Beste et al., 2001; Bozzini et al., 2004; Hussainova et al., 2014; Xia et al., 2016; Zhang et al., 2017; Liu et al., 2018). For applications for cutting tools, because the highest temperature at tool/chip interface may vary between 600 and 1000°C (Bhaumik et al., 1999; Majumdar et al., 2005; Sutter and Ranc, 2007), oxidation of cemented carbides will take place in dry and high speed cutting (Basu and Sarin, 1996; Voitovich et al., 1996; Campo et al., 2009; Chen et al., 2015; Chen et al., 2016), which will result in the degradation of mechanical properties and decreasing of their service lifetime. Literatures show that oxidation occur

preferentially in the Co binder phase (Voitovich et al., 1996; Chen et al., 2015; Chen et al., 2016). In the work of Chen et al. (Chen et al., 2015; Chen et al., 2016), it is reported that WC-Co cemented carbides have the selective oxidation characteristic at 500°C, results shown that the oxidation of Co phase was prior to the oxidation of WC phase. The O content in Co phase increases quickly while there is no change of O content in WC phase because no oxidation takes place.

Binderless tungsten carbide has received wide attention of scholars worldwide because of its higher hardness (Imasato et al., 1995; Tsai et al., 2010), better abrasion resistance and corrosion resistance (Engqvist et al., 1999; Beste et al., 2001; Hussainova et al., 2014; Wang et al., 2018) compared with the conventional tungsten carbide with metallic binder cobalt. To address the drawbacks such as the high sintering temperature, low density and poor fracture toughness of the binderless tungsten carbide, researchers have carried out extensive studies and proposed a variety of methods to lower the sintering temperature and improve the mechanical properties (Zheng et al., 2013; Ren et al., 2015; Kwak et al., 2016; Nino et al., 2017; Wang et al., 2018). Nevertheless, there have been few reports on the oxidation process of the binderless tungsten carbide. In our previous study (Wang et al., 2018), we found the addition of Y_2O_3 was of significant influence on the sintering densification and mechanical properties of binderless tungsten carbide. The hardness and fracture toughness of WC-1 wt.% Y_2O_3 increased by 46 and 40% compared to the pure WC. However, the effect of Y_2O_3 addition on high-temperature oxidation of binderless tungsten carbide is still unclear, which will affect the design and application of the binderless tungsten carbide as cutting tool materials.

The main purpose of the present work is to investigate the oxidation kinetics law of the binderless tungsten carbide with different contents of Y_2O_3, analyze the microstructure of the oxidation layer and discuss the oxidation mechanism of Y_2O_3 in binderless tungsten carbide.

EXPERIMENTAL PROCEDURE

The WC powder used in this research was supplied by Xiamen Golden Egret Special Alloy Co. Ltd., Xiamen, China, and the average grain size was 0.2 μm. To remove the surface oxide, WC powder was firstly pretreated with activated liquid consisting of 30 ml L^{-1} nitric acid (HNO_3), 40 ml L^{-1} hydrofluoric acid (HF) and 3 g L^{-1} ammonium fluoride (NH_4F). Then, the pretreated WC powder was used to prepare Y_2O_3-doped WC powder with Y_2O_3 contents of 1, 2, 3 and 4 wt.% by the chemical co-precipitation method. The specific process of activation pretreatment and preparation of Y_2O_3-doped WC powder were described in our previous study (Wang et al., 2018). The pure WC and Y_2O_3-doped WC were sintered with an SPS system produced by Sumitomo Coal Mining Co., Ltd. using a sintering temperature of 1600°C, sintering pressure of 45 MPa, a heating rate of 100°C/min and a holding time of 5 min. The YG3 cemented carbide used for comparative test was provided by Zhuzhou cemented carbide cutting tools co., Ltd. The compositions of the WC cemented carbides are shown in **Table 1**.

The oxidation weight gain test was carried out in a tube furnace. Specimens for the experiment with the dimension of about 10 mm × 10 mm × 5 mm were cut from the sintered samples. The surfaces of the specimens were ground and polished. Before the oxidation experiment, we measured the length and width of each surface of the specimens with a spiral micrometer with an accuracy of 0.01 mm, and then calculated the surface area. The specimens were placed in a tube furnace and were heated to the oxidizing temperature at a heating rate of 10°C/min, and the oxidizing temperature was held for a certain time before cooling off. Oxidizing temperatures of 600°, 700°, 750° and 800°C, and holding times of 30, 60, 90 and 120 min were used. The specimens before and after the oxidation were weighed using an analytical balance with an accuracy of 1×10^{-4}g, each sample was measured five times and averaged. The fracture and surface of the oxidation layers were observed by field emission scanning electron microscopy (FE-SEM, Model: S-4800, Hitachi, Japan). The composition and phase of the oxidation products were analyzed by energy dispersive spectrometry (EDS) and X-ray diffraction (XRD, Model: D8-Advance, Germany) analysis. The electron cloud density of binderless tungsten carbide's oxidation atom ball-and-stick model was simulated by Guassion09W software.

RESULTS AND DISCUSSION

Oxidation Kinetics

The oxidation resistance of the WC cemented carbide was determined by measuring the weight change after the oxidation at the temperatures of 600°, 700°, 750 ° and 800°C respectively. The weight gains per unit surface area of the WC cemented carbide vs. oxidized time at different temperatures were shown in **Figure 1**. **Figure 1A** shows the weight gain of the WC cemented carbide oxidized at 600°C for 120 min. It is observed that both the binderless tungsten carbide with different contents of Y_2O_3 and the YG3 cemented carbide show a small weight increase during oxidation at 600°C. However, the binderless tungsten carbide specimen with 1 wt.% Y_2O_3 has the smallest oxidation weight gain of 0.097 mg cm^{-2} while the oxidation weight gain of the YG3 cemented carbide sample is 1.62 mg cm^{-2} for the same oxidation condition. **Figures 1B–D** shows the oxidation kinetics curves of different WC cemented carbide at the oxidation temperatures of 700°C, 750°C and 800°C,

TABLE 1 | Compositions of WC cemented carbides (wt.%).

WC cemented carbide	WC wt.%	Y_2O_3 wt.%	Co wt.%
WC	100	—	—
WC-1 wt.% Y_2O_3	99	1	—
WC-2 wt.% Y_2O_3	98	2	—
WC-3 wt.% Y_2O_3	97	3	—
WC-4 wt.% Y_2O_3	96	4	
YG3	97	—	3

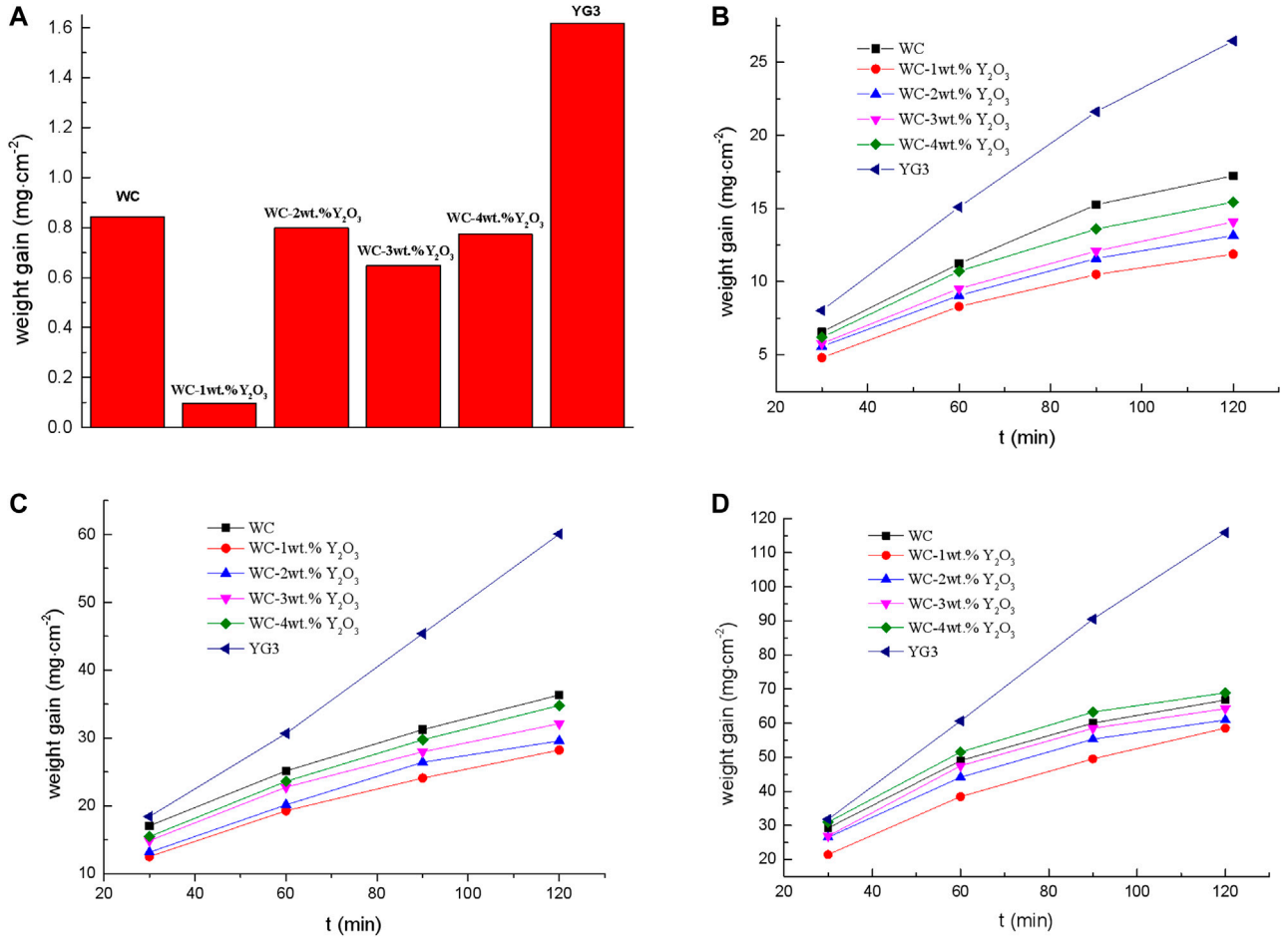

FIGURE 1 | Oxidation weight gain of YG3 cemented carbide and binderless tungsten carbide with different contents of Y_2O_3 at different oxidation temperatures. **(A)** 600°C, 120 min. **(B)** 700°C. **(C)** 750°C. **(D)** 800°C.

respectively. It can be seen from the oxidation dynamics curve that the weight gain rate of YG3 cemented carbide does not change with the increase in the oxidation time, and the antioxidant performance is poor. However, as the oxidation time increases, the oxidation weight gain of all binderless tungsten carbide specimens with different contents of Y_2O_3 tends to slow down and the oxidation rate gradually decreases, which demonstrates that the antioxidant capacities of binderless tungsten carbides are better than that of YG3 cemented carbide. A comparison between **Figures 1A,B** shows that the oxidation weight gain rate of WC cemented carbide at 700 °C increased by one to two orders of magnitude compared to that at 600°C. As can be seen from **Figures 1B,C** binderless tungsten carbide with 1 wt.% Y_2O_3 oxidation shows the smallest weight gain and thus has the best antioxidant ability. With the increase of the Y_2O_3 content, the oxidation weight gain of the binderless tungsten carbide increases gradually, and the antioxidant capacity decreases; nevertheless, all samples show better antioxidant capacity than that of pure WC. For the oxidation temperature of 800°C, the antioxidant capacity of WC-4 wt.% Y_2O_3 decreased significantly, while that of WC-1 wt.% Y_2O_3 remained adequate (**Figure 1D**). The oxidation weight gain of the YG3 cemented carbide sample oxidized at 800°C for 120 min was 111.87 mg cm^{-2}, while that of WC-1wt.% Y_2O_3 was only 58.54 mg cm^{-2}, corresponding to a decrease of 47.7% compared with the YG3 cemented carbide sample.

When the high-temperature oxidation kinetics curve of the material conforms to the parabolic law, it can be expressed by the following formula (Tatarko et al., 2013):

$$\Delta m^2 = kt + C \quad (1)$$

$$k = k_0 \exp(-Q/RT) \quad (2)$$

where Δm is the mass change per unit surface area, mg cm^{-2} ; t is the oxidation time, min; k is the parabolic oxidation rate constant, $mg^2 \cdot cm^{-4} s^{-1}$; C is the constant that accounts for the initial reaction; k_0 is a constant; Q is the oxidative activation energy, kJ mol^{-1}; T is the oxidizing temperature, K; and R is the gas constant.

According to the test data in **Figure 1**, square of oxidation weight gain of binderless tungsten carbide vs. time at different oxidation temperatures was drawn and basically close to a

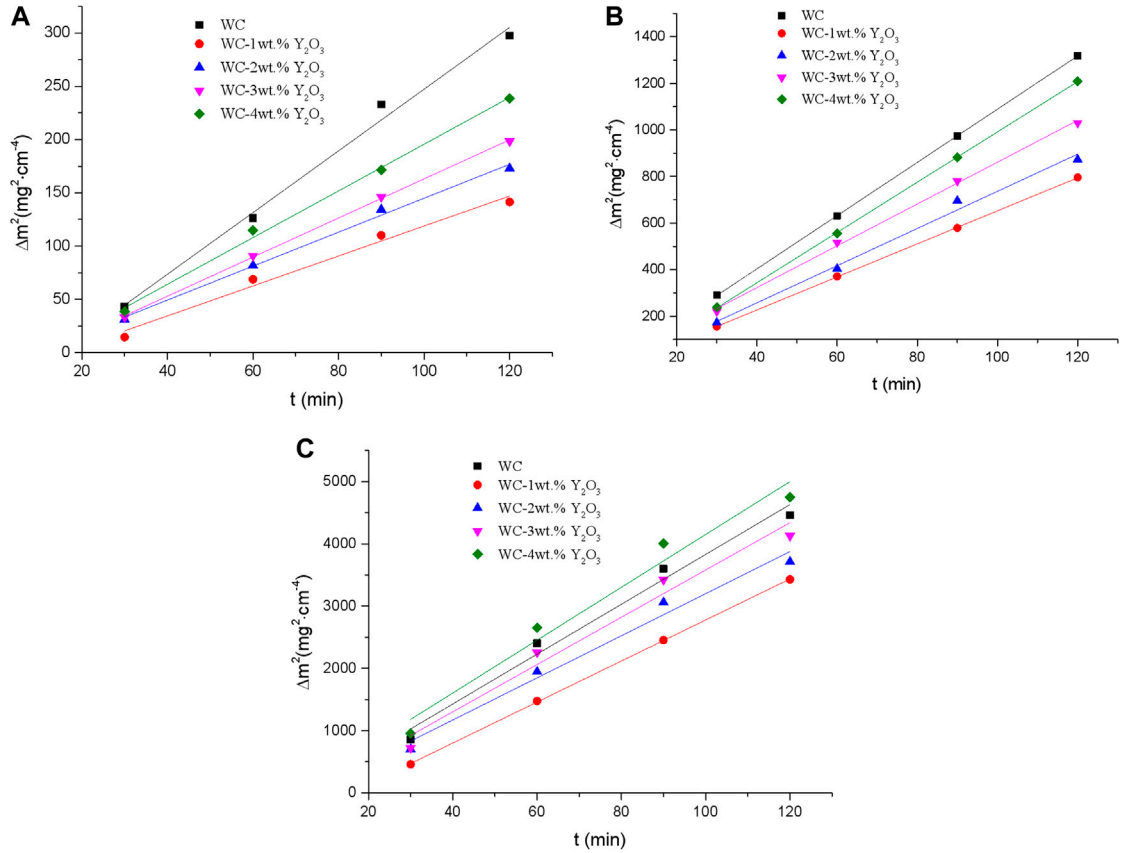

FIGURE 2 | Square of oxidation weight gain of binderless tungsten carbide vs. time at different oxidation temperatures. **(A)** 700°C; **(B)** 750°C; **(C)** 800°C.

TABLE 2 | *k* and *Q* values of binderless tungsten carbide with different Y_2O_3 contents.

Binderless tungsten carbide	k/mg^2 cm^{-4}·s^{-1}			Q/kJ mol^{-1}
	700°C	750°C	800°C	
WC	4.83 × 10^{-2}	1.90 × 10^{-1}	6.67 × 10^{-1}	237
WC-1 wt.% Y_2O_3	2.34 × 10^{-2}	1.18 × 10^{-1}	5.49 × 10^{-1}	285
WC-2 wt.% Y_2O_3	2.65 × 10^{-2}	1.33 × 10^{-1}	5.63 × 10^{-1}	275
WC-3 wt.% Y_2O_3	3.06 × 10^{-2}	1.50 × 10^{-1}	6.33 × 10^{-1}	271
WC-4 wt.% Y_2O_3	3.65 × 10^{-2}	1.81 × 10^{-1}	7.07 × 10^{-1}	262

straight line (**Figure 2**). That means the oxidation kinetics curve of binderless tungsten carbide oxidized in the temperature range from 700° to 800°C are consistent with the parabolic law. Using **Eq. 1**, the values of the parabolic oxidation rate constant *k* were estimated from the slopes of the square of the weight gain per unit surface area plotted vs. time. The oxidative activation energy *Q* was calculated from the slope of the Arrhenius plot between the parabolic rate constants and the oxidation temperatures. The values of the parabolic oxidation rate constant *k* and the oxidative activation energy *Q* in the temperature range from 700° to 800°C were calculated, and the results are shown in **Table 2**. An examination of the data presented in **Table 2** shows that the value of the parabolic oxidation rate constant *k* of binderless tungsten carbide with Y_2O_3 addition is smaller than that of pure WC for all temperatures in the 700°–800°C range, while the values of the oxidation activation energy *Q* are larger than those of pure WC. As the Y_2O_3 content increased from 1 to 4 wt.%, the value of the oxidation rate constant *k* gradually increased, and the activation energy *Q* gradually decreased. The oxidation rate constant *k* reflects the antioxidant performance, and oxidation is a thermal activation process, so that the oxidation activation energy *Q* represents the energy barrier that must be crossed during oxidation, and indicates the difficulty of oxidation. Thus, better oxidation resistance is obtained for smaller values of *k* and bigger values of *Q*. The addition of Y_2O_3 in the binderless tungsten carbide increases the energy needed for oxidation reaction, and improves the oxidation resistance of binderless tungsten carbide. However, with the increase in the Y_2O_3 content, the oxidation resistance of binderless tungsten carbide gradually declines.

TABLE 3 | Oxidation reaction equations and corresponding change of Gibbs free energy (ΔG) in WC-Y_2O_3 cemented carbide.

No	Oxidation reaction equation	ΔG of reaction
(1)	$2/5WC(s) + O_2(g) = 2/5WO_3(s) + 2/5CO_2(g)$	$\Delta G = -476{,}760 + 98.3\,T$
(2)	$2/5WC(s) + 2/5Y_2O_3(s) + O_2(g) = 2/5Y_2WO_6\,(s) + 2/5CO_2\,(g)$	$\Delta G = -536{,}480 + 104.4\,T$

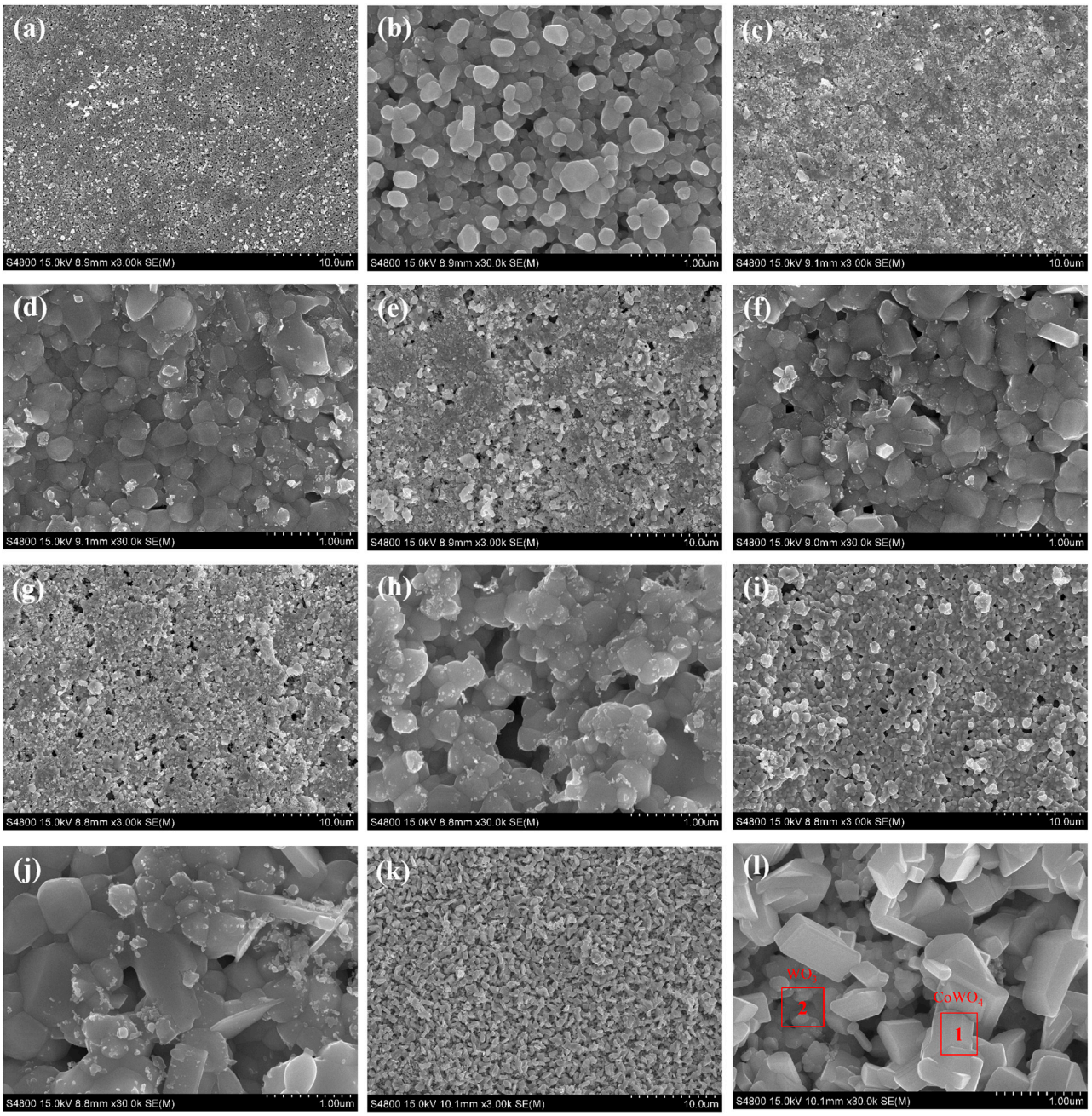

FIGURE 3 | Surface morphology of the oxidation layer of binderless tungsten carbide with different Y_2O_3 contents and YG3 cemented carbide oxidized at 800°C for 60 min **(A,B)** WC; **(C,D)** WC-1 wt.% Y_2O_3; **(E,F)** WC-2 wt.% Y_2O_3; **(G,H)** WC-3 wt.% Y_2O_3; **(I,J)** WC-4 wt.% Y_2O_3 **(K,L)** YG3.

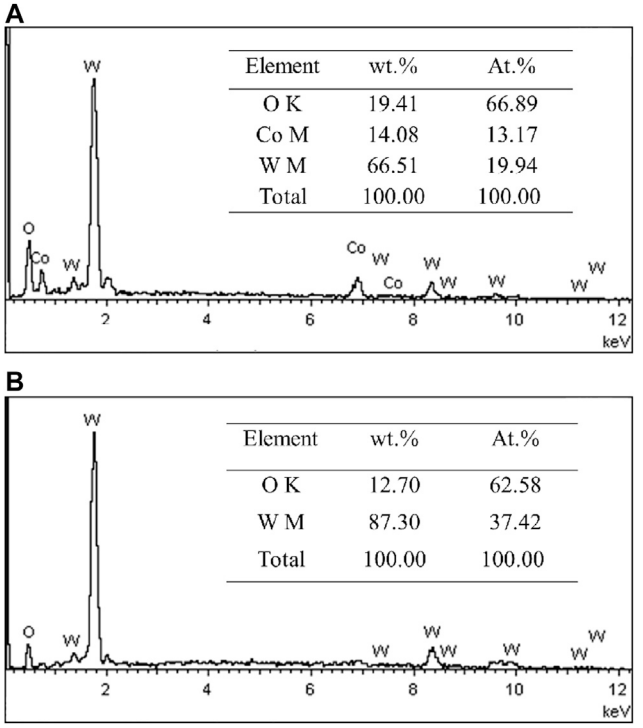

FIGURE 4 | EDS analysis results of micro zones 1 **(A)** and 2 **(B)** of YG3 shown in **Figure 2L**.

Observation and Analysis of Oxidized Surfaces and Cross-Sections

Figure 3 presents the surface morphologies of the oxidation layer of binderless tungsten carbide with different Y_2O_3 contents and of YG3 cemented carbide that are oxidized at 800°C for 60 min. **Figure 3A,B** show that there are many pores uniformly distributed on the surface of the oxidation layer of pure tungsten carbide and the grains are loose. However, the addition of Y_2O_3 in binderless tungsten carbide greatly improves the compactness of the surface of the oxidation layer (**Figures 3C–J**); in particular, when the Y_2O_3 content is 1 wt.%, the surface of the oxidation layer is the densest, and hardly any pores are observed (**Figures 3C,D**). As the Y_2O_3 content increases, the grain size in the oxidation layer and the number of the pores increase gradually (**Figures 3E–J**). **Figures 3K,L** present the surface morphology of the oxidation layer of YG3 cemented carbide. The grain size varies greatly, and the space between the grains is relatively loose. The outer grains have regular multilateral shapes, while the inner grain is almost spherical (**Figures 3K,L**). The elemental composition of the oxidation surface of binderless tungsten carbide was analyzed via EDS. Due to the low Y_2O_3 content, only O and W elements were detected, whereas Y was not detected. **Figure 4** shows the results of the EDS analysis of the micro zones 1 and 2 of YG3 cemented carbide shown in **Figure 3L**. Zone 1 in **Figure 3L** has high Co element content (**Figure 4A**) while zone 2 only contains elements O and W with no Co (**Figure 4B**). Further XRD analysis was performed on the oxidation surface of YG3 cemented carbide as shown in **Figure 5A**. The WO_3 and $CoWO_4$ phases were detected on the surface of the oxidation layer of YG3 cemented carbide. According to the EDS and XRD results, the regular polygonal grain on the surface of the oxidation layer of YG3 is $CoWO_4$ and the almost spherical small grain is WO_3. **Figure 5B** shows the XRD results for the binderless tungsten carbide, which indicates that WO_3 is the major phase and that Y_2WO_6 is a secondary phase in the tungsten carbide with Y_2O_3.

Figure 6 displays the cross-section morphologies of different cemented carbide oxidized at 600°C for 30 min. It can be seen that YG3 has the thickest oxidation layer close to 10 μm, while pure WC is about 7 μm, and WC-1 wt.% Y_2O_3 has the thinnest oxidation layer with the thickness of less than 5 μm. In YG3 and pure WC samples (seen from **Figures 6A,B**), the interface between the oxidation layer and the substrate is not firm, and the peeling of the oxidation layer can be seen. However, the oxidation films of cemented carbides with Y_2O_3 are well combined with the substrate (seen from **Figures 6C,D**). When the content of Y_2O_3 increases from 2 to 4 wt.%, the thickness of the oxidation layer doesn't change much, ranging from 6 to 6.5 μm, and some micro cracks are distributed in the oxidation films (seen from the arrows in **Figures 6D–F**).

The above results indicate that the antioxidant performance of binderless tungsten carbide with 1 wt.% Y_2O_3 was found to be the best. To further observe the oxidation process of binderless tungsten carbide doped with Y_2O_3, the WC-1 wt.% Y_2O_3 fresh fracture was placed in a tube furnace, heated to the test temperature at a heating rate of 10°C/min, and then cooled after holding for 30 minat the test temperature. The test temperatures were 300°, 350°, 400°, 500° and 600°C. The fracture morphologies were observed by scanning electron microscopy. **Figure 7** shows the fracture morphologies of WC-1 wt.% Y_2O_3 oxidized at different temperatures. No oxidation phenomenon was observed at room temperature (**Figure 7A**) and at 300°C (**Figure 7B**). When the oxidation temperature was 350°C, partial oxidation occurs in the triangular area between the WC grains (indicated by the arrows in **Figure 7C**). With the further increase of the temperature from 400° to 600°C, the oxidation products gradually covered the entire section, and the oxidation products structure was dense (seen from **Figures 7D–F**).

DISCUSSION

The oxidation process is controlled by the interfacial reaction rate and the rate of the diffusion of the substances involved in the reaction through the oxidation layer. The oxidation rate curve of YG3 cemented carbide essentially increased linearly and the oxidation rate did not change with the thickening of the oxidation layer. The oxidation process of YG3 cemented carbide was controlled by the interface reaction and the oxidation resistance was poor. This is mainly because the oxidation products of YG3 cemented carbide are WO_3 and $CoWO_4$ with different grain sizes that give rise to a loose oxidation layer with cracks and faults and are not favourable for antioxidant protection. By contrast, the curve of the oxidation weight gain of binderless tungsten carbide conforms to the parabolic law, and the oxidation rate decreases with the increase of oxidation time. The oxidation reaction is mainly controlled by diffusion and the oxidation layer has good protective properties.

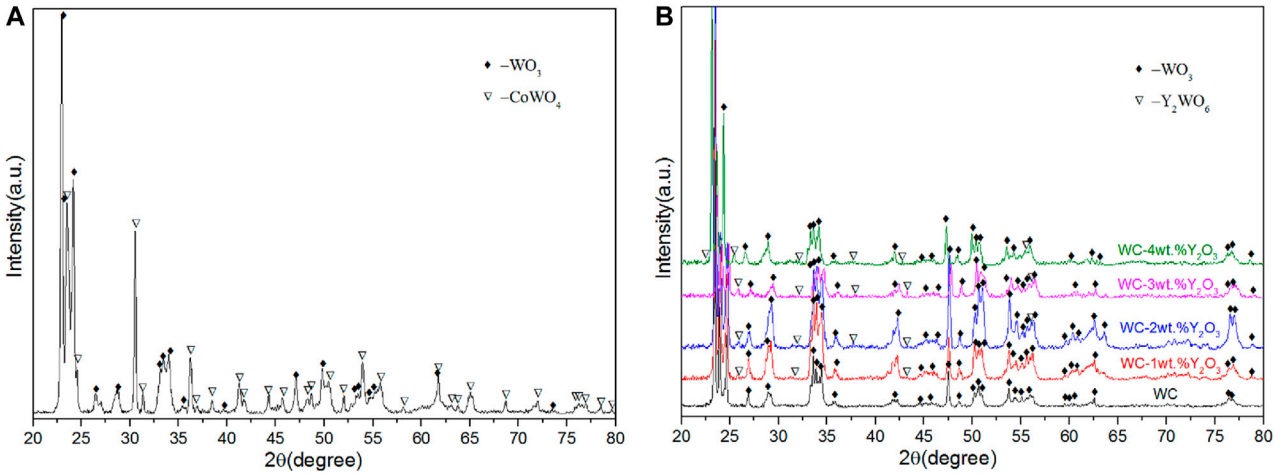

FIGURE 5 | XRD patterns of the surface of oxidation layer of YG3 cemented carbide **(A)** and binderless tungsten carbide with different Y_2O_3 contents **(B)**.

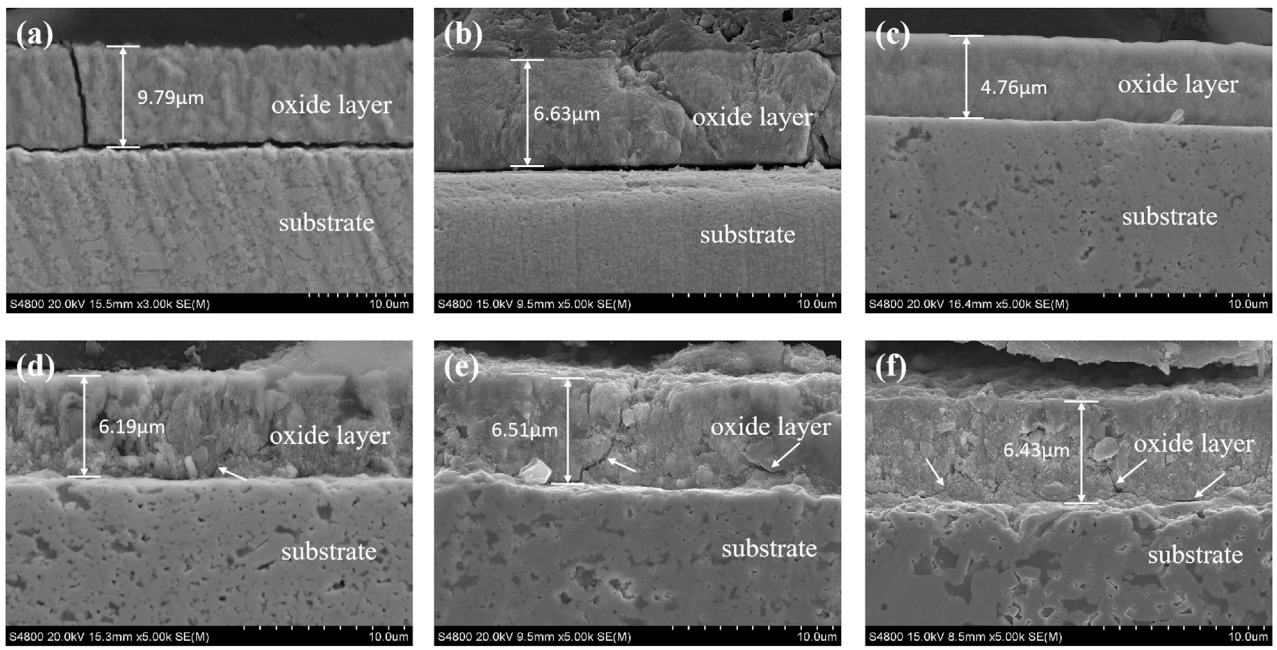

FIGURE 6 | Cross-section morphology of the different WC cemented carbides oxidized at 873 K for 30 min. **(A)** YG3; **(B)** pure WC; **(C)** WC-1 wt.% Y_2O_3; **(D)** WC-2 wt.% Y_2O_3; **(E)** WC-3 wt.% Y_2O_3; **(F)** WC-4 wt.% Y_2O_3.

The binderless tungsten carbide doped with Y_2O_3 has good oxidation resistance, we suggest as follows:

(1) Oxidation product Y_2WO_6 distributed at the triangle grain boundaries prevents the inward diffusion of O^{2-} and the outward diffusion of W^{4+}.

Figure 8 displays the SEM surface morphology (**Figure 8A**) and elemental analysis (**Figures 8B,C**) of WC-4wt.% Y_2O_3. It can be seen that element yttrium is mainly distributed at the WC triangle grain boundaries indicated by the arrows in **Figure 8A**. Combined with the XRD pattern of WC-4wt.% Y_2O_3 (**Figure 9**), the element yttrium exists in the form of Y_2O_3 phase. The ionic radius of Y^{3+} (0.090 nm) is much larger than that of W^{4+} (0.066 nm), and therefore, it is difficult for Y_2O_3 to form a solid solution with WC, so that Y_2O_3 is present mainly in the WC grain boundaries, which is consistent with the results in literature (Liu et al., 2015; Jin et al., 2017; He et al., 2018). Oxidation reaction equations and corresponding change of Gibbs free energy (ΔG) in WC-Y_2O_3 cemented carbide are

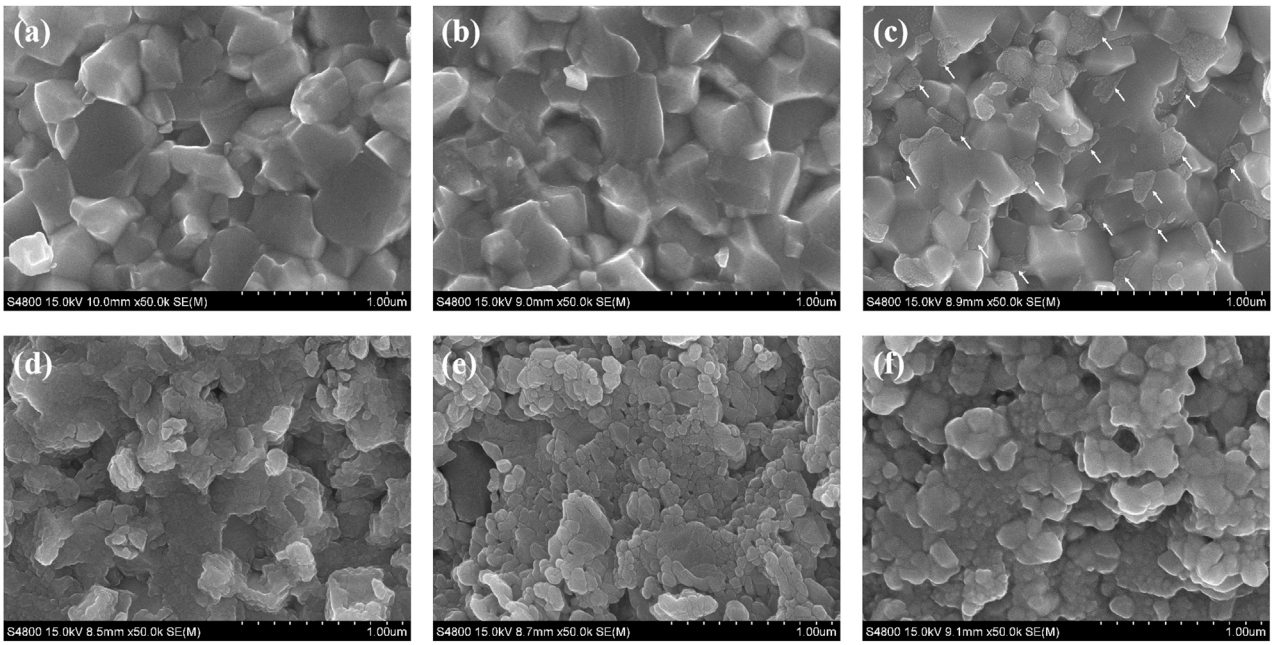

FIGURE 7 | SEM images of the fracture surface of WC-1wt.% Y_2O_3 oxidized at different temperatures. **(A)** original; **(B)** 300°C; **(C)** 350°C; **(D)** 400°C; **(E)** 500°C; **(F)** 600°C.

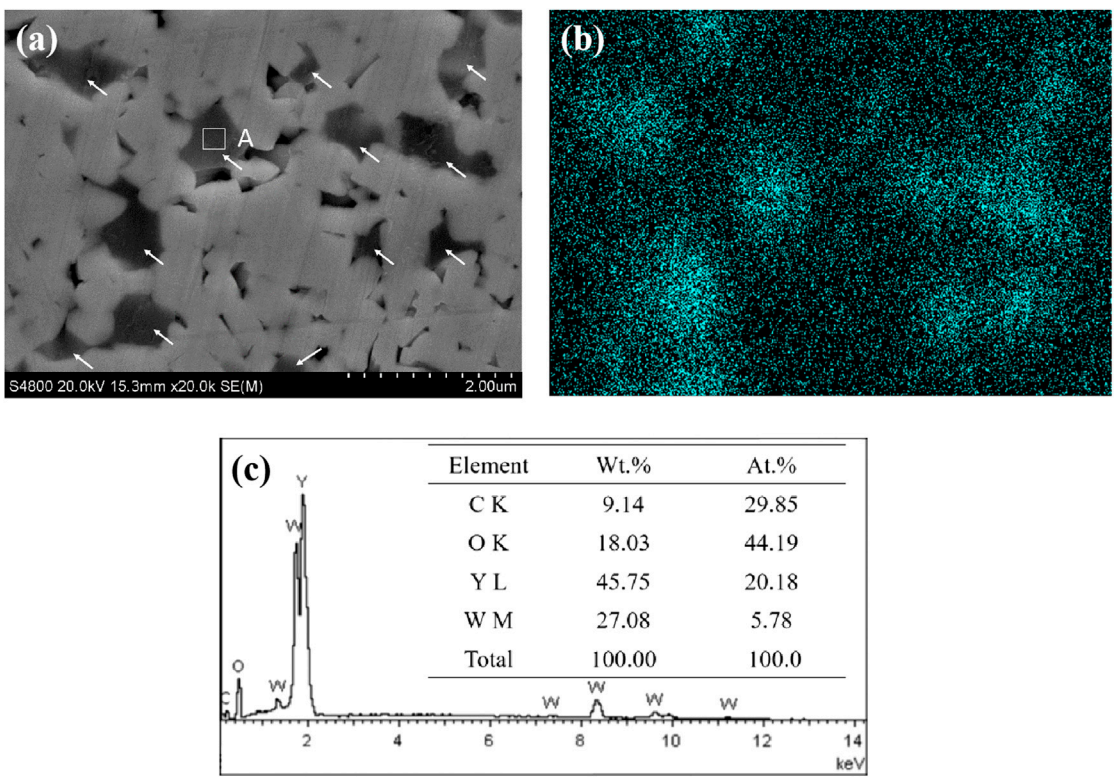

Element	Wt.%	At.%
C K	9.14	29.85
O K	18.03	44.19
Y L	45.75	20.18
W M	27.08	5.78
Total	100.00	100.0

FIGURE 8 | SEM surface morphology **(A)** and elemental analysis of WC-4wt.% Y_2O_3 **(B,C)**. **(B)** The distribution of yttrium in Panel **(A)**; **(C)** EDS analysis result of micro zone A in Figure. a.

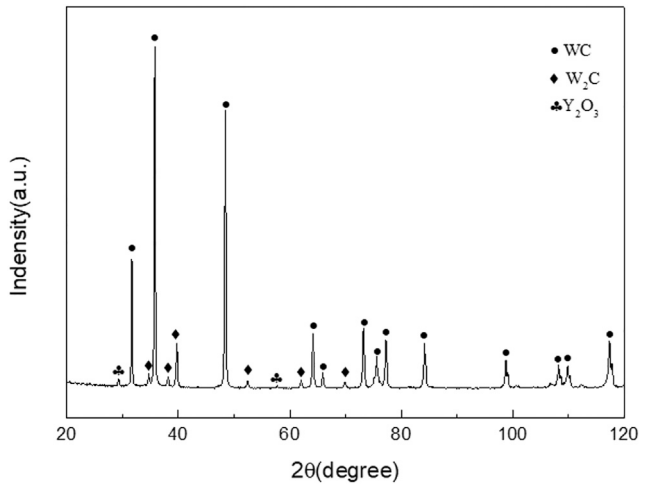

FIGURE 9 | XRD pattern of WC-4wt.% Y_2O_3.

shown in **Table 2**. **Figure 10** shows the ΔG–T relation curves of each reaction according to **Table 2**. It can be seen from **Figure 10** that the Gibbs free energy of WC oxidation reaction with Y_2O_3 or not increases with the increase of temperature, but greatly reduced while with Y_2O_3, which means the greater thermodynamic trend. Therefore, in the high temperature oxidation process, WC in the triangle grain boundary was first oxidized to Y_2WO_6. When the compact WO_3 oxidation layer was formed with the bare WC, the growt.h of the oxidation layer is mainly determined by W^{4+} and O^{2-} diffusion velocities along the grain boundary. The presence of the Y_2WO_6 with the high ionic radius, the transport of W^{4+} outward along the grain boundary and the diffusion of O^{2-} inward along the grain boundary were hindered and thus the antioxidant capacity of binderless tungsten carbide was improved by the addition of Y_2O_3.

(1) The excellent adhesion between the oxidation layer and the substrate surface is enhanced with the "pinning effect" of Y_2WO_6.

Figure 11 shows the oxidation layer/substrate atom ball-and-stick model (Zhong et al., 2015; Zhong et al.,2019) of pure WC and WC-Y_2O_3 cemented carbide, and the simulation calculation diagram of electron cloud density of frontier molecular orbits (HOMO and LUMO) of the two models calculated based on Guassion09W software. As can be seen from the atomic model in **Figure 11A**, WO_3 oxidation layer is formed after pure WC oxidized. Electron cloud density simulation diagram in **Figure 11B** shows that there is no enrichment of electron cloud between atoms 4C and 1W in HOMO and LUMO frontier molecular orbits, which proves that the adhesion between WO_3 oxidation layer and WC substrate is poor and WO_3 oxidation layer is easy to fall off. In the atomic model doped with Y_2O_3 in **Figure 11C**, Y_2O_3 and WO_3 are easy to oxidize to form a more stable Y_2WO_6 phase (seen from **Figure 10**). Since Y (electronegativity: 1.22) is the least electronegative atom than W (electronegativity: 2.36) and C (electronegativity: 2.55) atoms, part of the charge of Y atom will be transferred to atoms W-C, a certain degree of electron cloud enrichment can be clearly seen between atoms 4C and 1W in HOMO and LUMO frontier molecular orbits in **Figure 11D**, improving the adhesion between the Y_2WO_6 oxidation layer and WC substrate. The excellent adhesion between the oxidation layer and the substrate surface is enhanced with the "pinning effect" of Y_2WO_6 (Pint, 1996; Sun et al., 2016; Yu et al., 2017), which

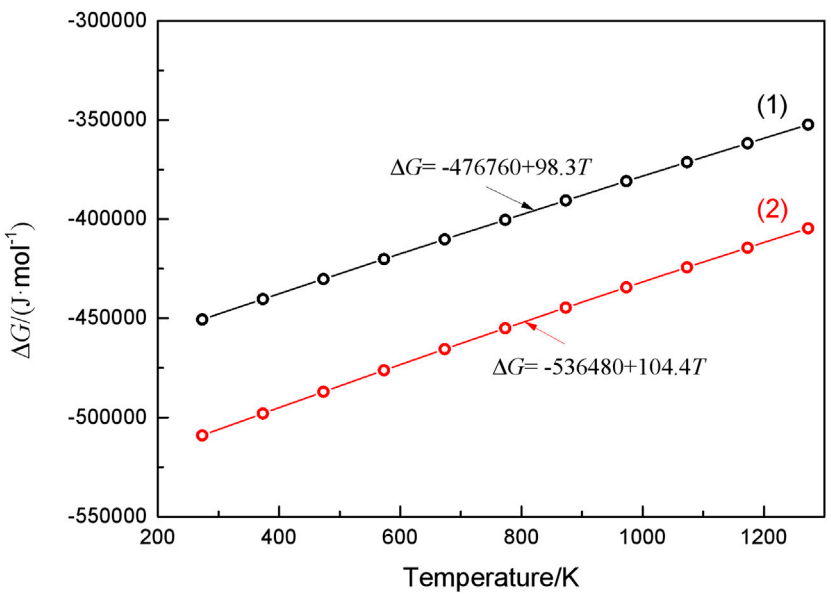

FIGURE 10 | The change in Gibbs free energy (ΔG) for the oxidation of component in WC-Y_2O_3 cemented carbide.

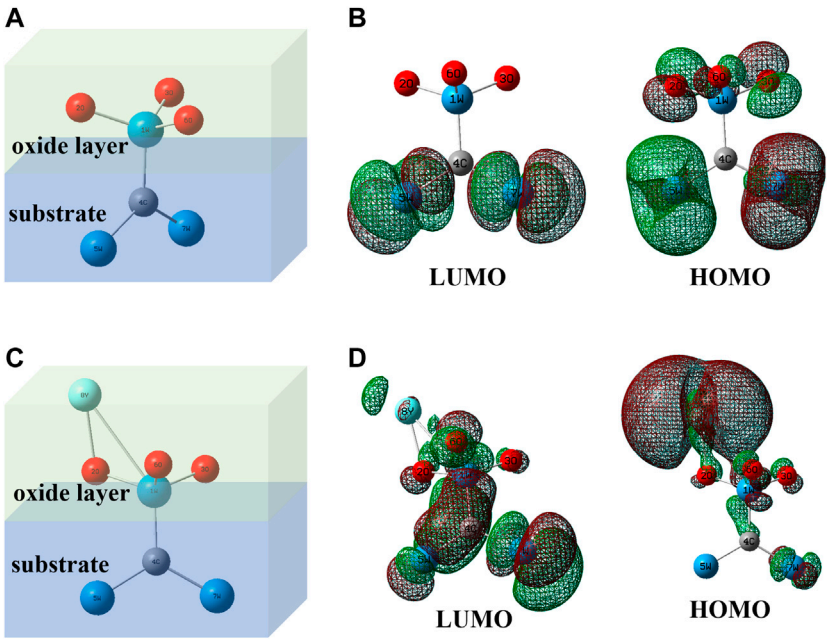

FIGURE 11 | Simplified oxidation layer/substrate atomic ball-and-stick models of and their electron cloud density simulation diagram. **(A)** WO_3/WC; **(B)** frontier molecular orbits of model **(A)**; **(C)** Y_2WO_6/WC; **(D)** frontier molecular orbits of model **(C)**.

also leads to the improvement of the oxidation resistance. However, with the increase in the Y_2O_3 content, the local enrichment of Y_2O_3 results in the local rapid oxidation of tungsten carbide and overflows a large amount of CO and CO_2 gases. A large outflow of gases resulted in the presence of defects such as pores or cracks (seen from **Figures 3**, **6**), which promotes oxidation rate and reduces the antioxidant capacity of binderless tungsten carbide. The oxidation resistance of binderless tungsten carbide with 1 wt.%Y_2O_3 is the best among the samples with different content of Y_2O_3.

CONCLUSION

The effects of Y_2O_3 addition on high temperature oxidation of binderless tungsten carbide were investigated. The conclusions are as follows: The addition of Y_2O_3 to the binderless tungsten carbide decreased the oxidization rate constant *k* and increased the oxidation activation energy *Q*, which means that the antioxidant property of binderless tungsten carbide was greatly improved with the addition of Y_2O_3. Meanwhile, the adhesion between the oxidation layer and the substrate surface is enhanced with the addition of Y_2O_3. With the Y_2O_3 content increasing from 1 to 4 wt.%, the antioxidant properties of binderless tungsten carbide gradually declined but were still better for all cases than those of pure tungsten carbide and YG3 cemented carbide. After oxidation at 800°C for 120 min, the oxidation weight gain of YG3 cemented carbide was 111.87 mg cm^{-2}, while that of WC-1 wt.% Y_2O_3 was only 58.54 mg cm^{-2}, corresponding to the reduction by 47.7% compared to YG3 cemented carbide.

DATA AVAILABILITY STATEMENT

The original contributions presented in the study are included in the article/Supplementary Material, further inquiries can be directed to the corresponding authors

AUTHOR CONTRIBUTIONS

JW has made substantial contributions to the data collection and writing of this work. DZ and LZ have made significant contributions to the framework design. ZT, WL and XZ were involved in the data analysis and discussions. XL and YW have helped with the data testing. All authors listed have made a substantial, direct, and intellectual contributions to the work, and approved it for publication.

FUNDING

This research was supported by the National Nature Science Foundation of China, grant number 21671145; Funding of Jiangsu Innovation Program for Graduate Education, grant number KYLX_0228; and Zhejiang Provincial Key Laboratory for Cutting Tools, grant number ZD201610.

REFERENCES

Basu, S. N., and Sarin, V. K. (1996). Oxidation behavior of WC–Co. *Mater. Sci. Eng. A.* 209, 206–212. doi:10.1016/0921-5093(95)10145-4

Beste, U., Hammerström, L., Engqvist, H., Rimlinger, S., and Jacobsona, S. (2001). Particle erosion of cemented carbides with low Co content. *Wear* 250, 809–817. doi:10.1016/S0043-1648(01)00735-9

Bhaumik, S. K., Balasubramaniam, R., Upadhyaya, G. S., and Vaidya, M. L. (1999). Oxidation behaviour of hard and binder phase modified WC–10 Co cemented carbides. *J. Mater. Sci. Lett.* 11, 1457–1459. doi:10.1007/BF00729663

Bozzini, B., Gaudenzi, G. P. D., Fanigliulo, A., and Mele, C. (2004). Electrochemical oxidation of WC in acidic sulphate solution. *Corros. Sci.* 46, 453–469. doi:10.1016/S0010-938X(03)00146-X

Campo, L. D., Pérez-Sáez, R. B., González-Fernández, L., and Tello, M. J. (2009). Kinetic sinversion in isothermal oxidation of uncoated WC-based carbides between 450 and 800°C. *Corros. Sci.* 51, 707–712. doi:10.1016/j.corsci.2008.12.022

Chen, L., Yi, D. Q., Wang, B., Liu, H. Q., Wu, C. P., Huang, X., et al. (2015). The selective oxidation behaviour of WC-Co cemented carbides during the early oxidation stage. *Corros. Sci.* 94, 1–5. doi:10.1016/j.corsci.2015.02.033

Chen, L., Yi, D., Wang, B., Liu, H. Q., and Wu, C. P. (2016). Mechanism of the early stages of oxidation of WC-Co cemented carbides. *Corros. Sci.* 103, 75–87. doi:10.1016/j.corsci.2015.11.007

Engqvist, H., Axén, N., and Hogmark, S. (1999). Tribological properties of a binderless carbide. *Wear* 232, 157–162. doi:10.1016/S0043-1648(99)00140-4

He, W., Tan, D. Q., Kuang, H., Li, Y. L., Yang, X., and Zhu, H. B. (2018). Effect of yttrium barrier on the preparation of precursor powders of WC-Co cemented carbide and properties of sintered bulk. *J. Alloys Compd.* 742, 702–711. doi:10.1016/j.jallcom.2018.01.379

Hussainova, I., Antonov, M., Voltsihhin, N., and Kübarsepp, J. (2014). Wear behavior of Co-free hardmetals doped by zirconia and produced by conventional PM and SPS routines. *Wear* 312, 83–90. doi:10.1016/j.wear.2014.01.014

Imasato, S., Tokumoto, K., Kitada, T., and Sakaguchi, S. (1995). Properties of ultra-fine grain binderless cemented carbide 'RCCFN'. *Int. J. Refract. Met. Hard Mater.* 13, 305–312. doi:10.1016/0263-4368(95)92676-B

Jin, H., Shi, Z. Q., Li, X. D., Li, Y. F., Xia, H. Y., Xu, Z., et al. (2017). Effect of rare earth oxides on the microstructure and properties of mullite/hBN composites. *Ceram. Int.* 43, 3356–3362. doi:10.1016/j.ceramint.2016.11.179

Kim, H. C., Oh, D. Y., and Shon, I. J. (2004). Synthesis of WC and dense WC-x vol.% Co hard materials by high-frequency induction heated combustion method. *Int. J. Refract. Met. Hard Mater.* 22, 41–49. doi:10.1016/j.ijrmhm.2003.12.002

Kwak, B. W., Song, J. H., Kim, B. S., and Shon, I. J. (2016). Mechanical properties and rapid sintering of nanostructured WC and WC-$TiAl_3$ hard materials by the pulsed current activated heating. *Int. J. Refract. Met. Hard Mater.* 54, 244–250. doi:10.1016/j.ijrmhm.2015.08.003

Liu, K., Wang, Z. H., Yin, Z. B., Cao, L. Y., and Yuan, J. T. (2018). Effect of Co content on microstructure and mechanical properties of ultrafine grained WC-Co cemented carbide sintered by spark plasma sintering. *Ceram. Int.* 44, 18711–18718. doi:10.1016/j.ceramint.2018.07.100

Liu, Y., Li, X. F., Zhou, J. H., Fu, K., Wei, W., Du, M., et al. (2015). Effects of Y_2O_3 addition on microstructures and mechanical properties of WC-Co functionally graded cemented carbides. *Int. J. Refract. Met. Hard Mater.* 50, 53–58. doi:10.1016/j.ijrmhm.2014.11.004

Majumdar, P., Jayaramachandran, R., and Ganesan, S. (2005). Finite element analysis of temperature rise in metal cutting processes. *Appl. Therm. Eng.* 25, 2152–2168. doi:10.1016/j.applthermaleng.2005.01.006

Nino, A., Nakaibayashi, Y., Sugiyama, S., and Taimatsu, H. (2017). Effect of Mo_2C addition on the microstructures and mechanical properties of WC-SiC ceramics. *Int. J. Refract. Met. Hard Mater.* 64, 35–39. doi:10.1016/j.ijrmhm.2016.12.018

Ou, X. Q., Xiao, D. H., Shen, T. T., Song, M., and He, Y. H. (2012). Characterization and preparation of ultra-fine grained WC-Co alloys with minor La-additions. *Int. J. Refract. Met. Hard Mater.* 31, 266–273. doi:10.1016/j.ijrmhm.2011.12.011

Pint, B. A. (1996). Experimental observations in support of the dynamic-segregation theory to explain the reactive-element effect. *Oxid. Met.* 45, 1–37. doi:10.1007/BF01046818

Ren, X. Y., Peng, Z. J., Wang, C. B., Fu, Z. Q., Qi, L. H., and Miao, H. Z. (2015). Effect of ZrC nano-powder addition on the microstructure and mechanical properties of binderless tungsten carbide fabricated by spark plasma sintering. *Int. J. Refract. Met. Hard Mater.* 48, 398–407. doi:10.1016/j.ijrmhm.2014.10.013

Sun, D. J., Liang, C. Y., Shang, J. L., Song, Y. R., Li, W. Z., Liang, T. Q., et al. (2016). Effect of Y_2O_3 contents on oxidation resistance at 1150°C and mechanical properties at room temperature of ODS Ni-20Cr-5Al alloy. *Appl. Surf. Sci.* 385, 587–596. doi:10.1016/j.apsusc.2016.05.143

Sutter, G., and Ranc, N. (2007). Temperature fields in a chip during high-speed orthogonal cutting-An experimental investigation. *Int. J. Mach. Tools Manu.* 47, 1507–1517. doi:10.1016/j.ijmachtools.2006.11.012

Tatarko, P., Kašiarová, M., Dusza, J., and Šajgalík, P. (2013). Influence of rare-earth oxide additives on the oxidation resistance of Si_3N_4 -SiC nanocomposites. *J. Eur. Ceram. Soc.* 33, 2259–2268. doi:10.1016/j.jeurceramsoc.2013.01.008

Tsai, K. M., Hsieh, C. Y., and Lu, H. H. (2010). Sintering of binderless tungsten carbide. *Ceram. Int.* 36, 689–692. doi:10.1016/j.ceramint.2009.10.017

Voitovich, V. B., Sverdel, V. V., Voitovich, R. F., and Golovko, E. I. (1996). Oxidation of WC-Co, WC-Ni and WC-Co-Ni hard metals in the temperature range 500–800°C. *Int. J. Refract. Met. Hard Mater.* 14, 289–295. doi:10.1016/0263-4368(96)00009-1

Wang, J. F., Zuo, D. W., Zhu, L., Li, W. W., Tu, Z. B., and Dai, S. (2018). Effects and influence of Y_2O_3 addition on the microstructure and mechanical properties of binderless tungsten carbide fabricated by spark plasma sintering. *Int. J. Refract. Met. Hard Mater.* 71, 167–174. doi:10.1016/j.ijrmhm.2017.11.016

Xia, X., Li, X. Q., Li, J. M., and Zheng, D. H. (2016). Microstructure and characterization of WC-2.8 wt.% Al_2O_3-6.8 wt.% ZrO_2 composites produced by spark plasma sintering. *Ceram. Int.* 42, 14182–14188. doi:10.1016/j.ceramint.2016.06.044

Xiao, D. H., He, Y. H., Song, M., Lin, N., and Zhang, R. F. (2010). Y_2O_3-and NbC-doped ultrafine WC-10Co alloys by low pressure sintering. *Int. J. Refract. Met. Hard Mater.* 28, 407–411. doi:10.1016/j.ijrmhm.2009.12.008

Yu, H., Ukai, S., Hayashi, S., and Oono, N. H. (2017). Effect of Cr and Y_2O_3 on the oxidation behavior of Co-based oxide dispersion strengthened superalloys at 900°C. *Corros. Sci.* 127, 147–156. doi:10.1016/j.corsci.2017.08.013

Zhang, L., Chen, Y., Zhang, H. D., Tang, W., and Zhou, L. (2017). Corrosion and strength degradation behaviors of binderless WC material and WC-Co hardmetal in alkaline solution: a comparative investigation. *Int. J. Refract. Met. Hard Mater.* 68, 1–8. doi:10.1016/j.ijrmhm.2017.06.003

Zhang, Q. L., To, S., Zhao, Q. L., Guo, B., and Wu, M. T. (2016). Effects of binder addition on the surface generation mechanism of WC/Co during high spindle speed grinding (HSSG). *Int. J. Refract. Met. Hard Mater.* 59, 32–39. doi:10.1016/j.ijrmhm.2016.05.005

Zheng, D. H., Li, X. Q., Li, Y. Y., Qu, S. G., and Yang, C. (2013). ZrO_2 (3Y) toughened WC composites prepared by spark plasma sintering. *J. Alloys Compd.* 572, 62–67. doi:10.1016/j.jallcom.2013.03.259

Zhong, A., Chen, D., and Li, L. (2015). Revisiting the beryllium bonding interactions from energetic and wavefunction perspectives. *Chem. Phys. Lett.* 633, 265–272. doi:10.1016/j.cplett.2015.06.007

Zhong, A., Jing, Y., Li, L., and Zhong, J. (2019). Theoretical study of metal ion impact on geometric and electronic properties of terbutaline compounds. *Monatsh. Chem.* 150, 1355–1364. doi:10.1007/s00706-019-02419-1

Conflict of Interest: Author XL was employed by the company Zhejiang Crystal-Optech Co. LTD.

The remaining authors declare that the research was conducted in the absence of any commercial or financial relationships that could be construed as a potential conflict of interest.